Application of the TISAR technique to the investigations of transportation facilities and detection of utilities

J.-L. Arsenault * and M. Chouteau **

* Géophysique GPR International Inc. ; École Polytechnique de Montréal
Longueuil, Qc., Canada ; jean-luc.arsenault@gprmtl.com
Montréal, Qc., Canada; jean-luc.arsenault@polymtl.ca

** École Polytechnique de Montréal
Montréal, Qc., Canada; Chouteau@geo.polymtl.ca

1- **Overview**

The use of frequency analysis of seismic data for shallow applications has been extensively investigated in the last decades. MASW and other methods related to surface waves, body waves and/or guided waves, are significant examples. Another approach is to use the vibratory frequency content information within the data, related to the geometry and the mechanical properties of a layer. The acronym "TISAR" stands for "Testing and Investigation using Seismo-Acoustic Resonance". It is then based on the analysis of the resonance frequencies of the structures under investigation when energized by a transient source. In practice, long recording from multiple seismic receivers allows time and spatial windowings, which are needed for an adequate extraction of the resonant frequencies; however processing is fairly simple.
Numerical modeling has shown it to be fairly indicative of the subsurface geometry and diverse applications have demonstrated its usefulness. In this paper, we show the TISAR technique to be very well adapted for sub-surface investigations such as the measurement of asphalt road thickness and the detection of utilities.

2- Introduction

The TISAR method was developed to complement traditional seismic methods within the well-known 0-10 m depth blind zone. The popular radar (or "GPR") method generally fills that gap quite efficiently. There are however two important limitations related to the radar technique: 1 – it is an electromagnetic method and it is not directly related to the mechanical properties of the material, and 2- it is non-operational over electrically conductive soils as ocean shores or clayey materials. The TISAR method was then set up to overcome these limitations, using seismic-acoustic signals. During the development of the method, we have realized it has wider applications than initially thought, especially for civil engineering NDT transportation facilities and infrastructures.

Numerical modeling has shown to be fairly indicative for the method possibilities considering the subsurface geometry, and diverse applications have demonstrated its usefulness. Some new approaches, interpretation basis and possible limitations were expected from the analysis of synthetic data. It could lead to a more efficient TISAR technique application.

Recent field applications have shown very promising results, some of them unexpected in comparison with the conventional geophysical / NDT methods. We believe that the TISAR method could be part of the new technologies for non-destructive testing in civil engineering.

3- Fundamental Concepts

The very first intention of this work was to extend the well-known "impact-echo" method to materials other than concrete and to larger scales. The main objective was to meet needs in geotechnical problems related to shallow and high resolution geological profiling (especially for foundations and pipe-lines routes studies) with an alternative seismic method.

3.1- **Principles of the impact-echo method**

In early '80s, the National Institute of Standards and Technology (NIST) of U.S.A., undertook the development of a method inspired from previous sonic recognized NDT methods for concrete evaluation. Few years after (1990), Dr Sansalone from Cornell University developed the actual (patented) method known as "impact-echo". This method is mainly used for defects detection inside simple concrete structures, and it is the subject of an ASTM norm (C 1383).

The "impact-echo" method principle stands on the assumption that a mechanical impact initiated at the surface of the investigated material, generates a transient compressional wave (P) which is reflected at the defect interface, toward the free surface, then reflected back down to the defect interface, etc. Considering the defect as a crack or a delamination within the concrete, it could be associated to "air" or a second free surface. The transient signal polarity is then reversed for every reflection causing the surface receiver to record the multiple reflections with a same polarity. Note that when the surface is impacted shear (S) and Rayleigh waves are generated in addition to P waves.

At the beginning of the study, the displacement of particles was considered (from an acoustic and ultra-sonic point of view) from a simple time perspective. It was then figured that an analysis in the frequency domain could be more efficient for a suitable data processing. The use of the Fast Fourier Transform (or "FFT") of the signals was then privileged as a tool for the identification of time-wise repetitive reflection signal of the acoustic wave, between the free surface and a reflective interface. The basic concept of the impact-echo method is illustrated at figure 1.

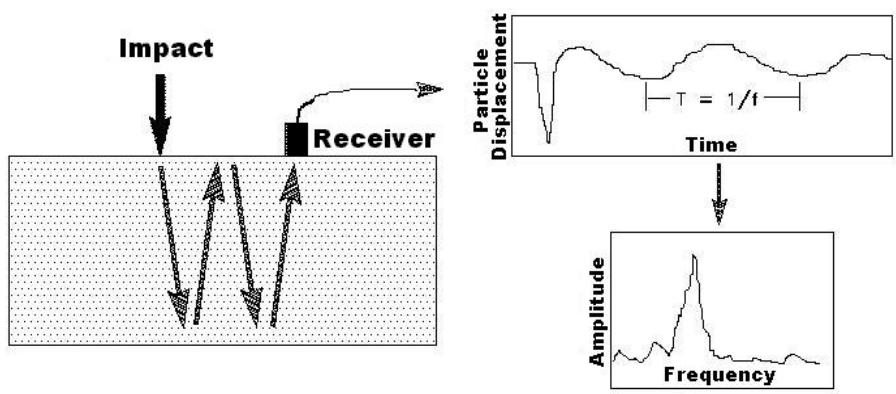

Figure 1. Schematic representation of the impact-echo method.

As presented in figure 1, after applying a transient signal to the surface, a receiver (located close to the impact point) records the particle displacement in time domain. The period of the multiple reflected waves is recognized by its corresponding frequency after a spectral analysis of the time record is realized. The material thickness can be evaluated from its seismic velocity "V" and the two way time reflection delay "T". Assuming a negligible distance between the impact point and the receiver location, one can consider that $T = t_{down} + t_{up,}$ and $t_{down} = t_{up,}$ which lead to the relation:

$$T = \frac{2H}{V} \quad \text{that can also be presented as } H = \frac{VT}{2} .$$

The multiple reflection delay "T" is known from its corresponding frequency, f = 1/T. The seismic velocity measured from the surface of the material is an apparent one, and as stated in the ASTM 1383, a correction factor of 0.96 should be applied to express the real seismic velocity. The thickness relation can therefore be written as:

$$H = \frac{V}{2f(0,96)} .$$

3.2- **Basics of TISAR**

Previous works have attempted to extend the impact-echo method to geological environments including unconsolidated sediments on surface. Most recent ones were conducted by Abraham (L.P.C.P., France) and Leonard (U. de Lille, France), from 1997 to 2000, but the results were deceiving. It must be noticed that these works rigorously respected the impact-echo requirements regarding the source-receiver distance. At Ecole Polytechnique of Montreal, since 1999, we have used a different approach.

The TISAR method somewhat differs from the impact-echo method by the data acquisition set-up and the processing operations. The TISAR method allows the solution of a multi-layers model, which could include increasing or decreasing acoustic impedance ("Z") layers with depth. As the acoustic impedances contrasts can be positive or negative, so can be the coefficient of reflection R_n (between layer n and n+1):

$$R_n = \frac{Z_{n+1} - Z_n}{Z_{n+1} + Z_n} \text{ where } Z_n = \rho_n V_n \text{ is the acoustic impedance of layer n.}$$

The thickness relation of the impact-echo method can be transformed and adapted to a multi-layers model.

$$H_n = V_n \left[\frac{1}{2 k_n f_n} - \sum_{i=1}^{n-1} \frac{H_i}{V_i} \right] \text{, where "}k_n\text{" ="1" for } Z_{n+1} < Z_n \text{, and "2" for } Z_{n+1} > Z_n.$$

The right-hand term inside the brackets is related to the seismic aspect of the recorded data, while the left-hand one is function of vibration behavior of the resonant layer. Similarly to the correction coefficient (0.96) of the impact-echo method, the left-hand term can be corrected with the expression:

$$\frac{\sqrt{12\left(1-\sigma_n^2\right)}}{\pi} \text{ , where "}\sigma\text{" is the Poisson ratio, also equal to } \frac{\frac{1}{2}\left(\frac{V_P}{V_S}\right)^2 - 1}{\left(\frac{V_P}{V_S}\right)^2 - 1}.$$

As the Poisson ratio for unconsolidated materials is usually within the range of 0.3 to 0.45, the correction coefficient would vary between 0,985 and 1,052. From a practical point of view, it can generally be neglected as assumed to be unitary.

To figure the main possibilities and limitations of the TISAR method, analysis of synthetic seismograms were done for various sub-surface layers, and different geometries. We used a commercial 2D finite difference software (FLAC from ITASCA). Figure 2 presents a synthetic seismogram generated for a simple model of 4 m thick moraine lying on bedrock, for which each trace is normalized according with the maximum amplitude of each trace. One can recognize the P (direct and refracted), the direct S and the Rayleigh waves, as well as guided waves, between the refracted P wave and the Rayleigh wave arrivals. The resonance signal appears clearly after the Rayleigh wave arrivals.

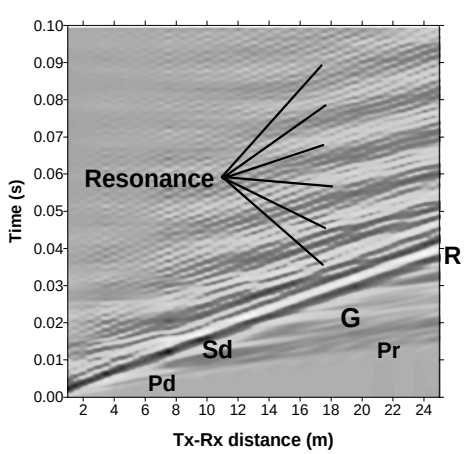

Figure 2. Synthetic seismogram with amplitude normalization.

The importance of the resonance signal is clearly visible at late time and at some distance from the shot point location.

Frequency analysis of the synthetic seismograms can be expressed as “f-x” spectrograms, displaying the normalized frequency content in function of the source-receiver (“Tx-Rx”) distance. Two simple models were used to verify the effect of the acoustic impedance contrast. The figure 3 shows the results for a 5 m thick moraine layer on bedrock (up) and a 5 m thick moraine layer on loose sand (down). The effect of the expected factor “2” related to “k” is demonstrated by the change of the resonant frequency 50 Hz compared to 100 Hz for cases 1 and 2 respectively. It is also interesting to observe a specific frequency signature related to the first case ($Z_1 < Z_2$), where frequency response increases with Tx-Rx distance, up to approximately Tx-Rx = H = 5 m, where it becomes independent of offset.

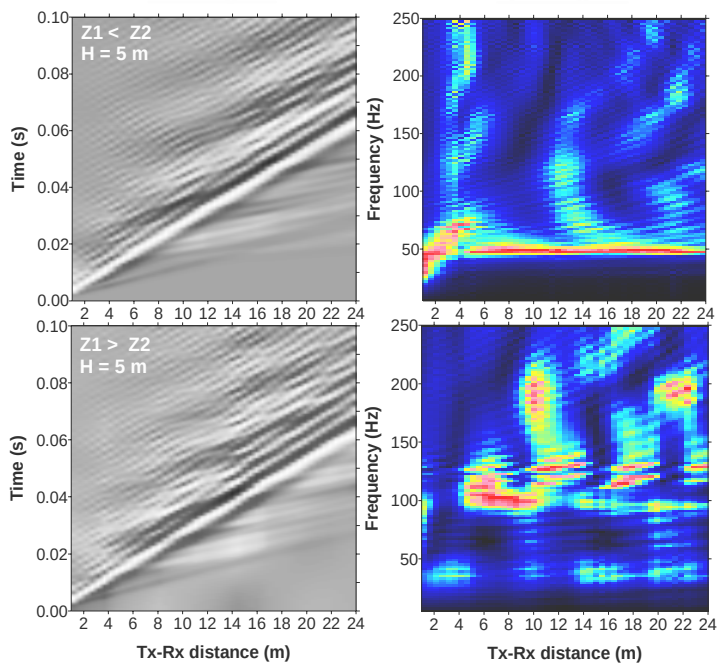

Figure 3. Synthetic seismograms and corresponding “f-x” spectrograms for increasing and decreasing acoustic impedance with depth.

The effect of increasing thickness of a dense moraine layer overlying bedrock, as along with the specific frequency signature for the case $Z_1 < Z_2$, is presented at figure 4. It presents the “f-x” spectrograms amplitude-normalized from trace to trace, calculated from synthetic seismograms.

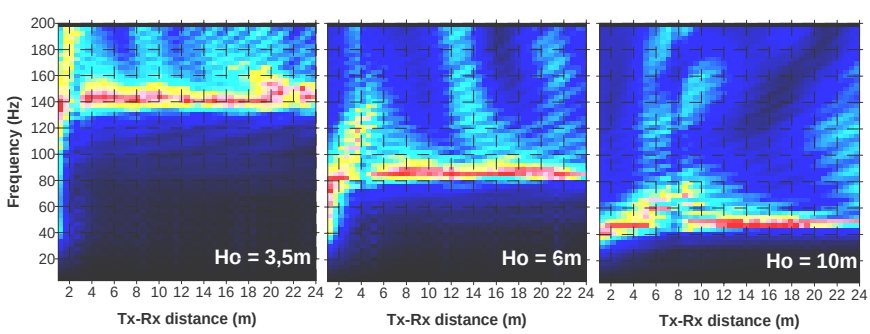

Figure 4. “f-x” spectrograms for increasing depth to positive acoustic impedance contrast.

If the velocity function of a layered material at a site is partly unknown, the use of the “f-x” spectrograms could allow to expect the nature of the “k” value (1 or 2); the presence of a specific frequency signature appearing in the vicinity of the shot point location (Tx-Rx < H) indicates an acoustic impedance increasing with depth.

A technique for the determination of the resonance frequency was previously proposed (Abraham, 1998 and Leonard, 2000) using a time windowing filter. This operation appears to yield good results for simple models, but it remains very tedious to apply for real cases, and it is very difficult to apply, especially for complex geometric cases. Figure 5 presents a continuous wavelet transform of the receiver located at Tx-Rx = 18 m relatively to figure 2. We propose to recognize the resonance frequency using a Tx-Rx distance windowing. Figure 6 illustrates a simple “f-x” spectrogram, where is it easy to exclude for subsequent processing phases the specific frequency signature appearing in the vicinity of the shot point location (Tx-Rx # H) and also to exclude the “long offset noise” frequency response. A simple adequate (and “optimum”) Tx-Rx distance window can then be chosen for further processing. This is the main point of the TISAR method, even if it violates the impact-echo method restrictions.

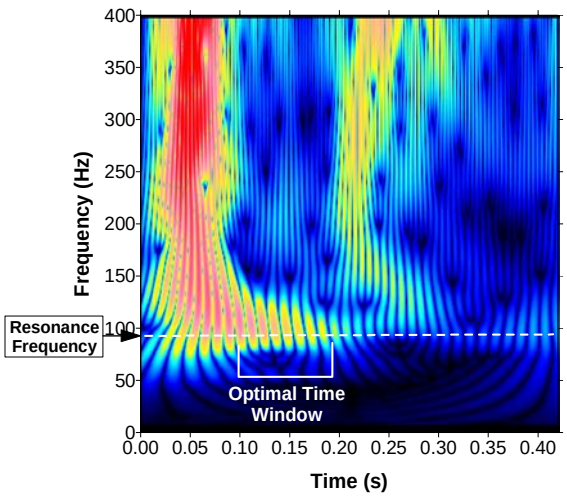

Figure 5. CWT scalogram transformed into an “f-x” spectrogram, showing the resonance frequency between the 90-190 ms time window.

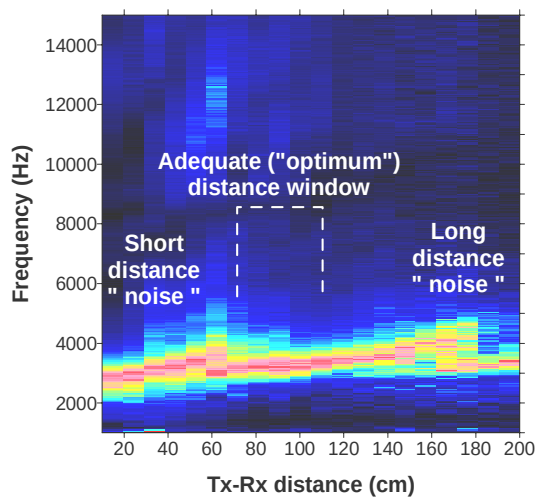

Figure 6. Experimental “f-x” spectrogram measured over asphalt paved road; adequate distance window is far from the source location.

4- Field Experiments

Even if the method is experimental, many field experiments were conducted with success in various environments and for different goals. The following examples are specifically relatives to roads assessment and shallow buried utilities detection.

4.1- Acoustic soundings on asphalt paved roads

Following a “GPR” asphalt thickness measurement campaign, physical calibrations on specific locations had to be performed for insurance and quality control. The actual case relates works performed in the Mauricie-Bois-Francs (Qc, Canada) during winter of 2001. The first step required for a complete TISAR survey is the seismic velocity measurement of the investigated materials. A modified Microsis© prototype was used for the measurement of the direct P wave through the asphalt. As presented at figure 7, it is composed of four piezoelectric receivers setted to 25 cm intervals. The source used was a conventional hammer impacted on the asphalt surface and records were done with a time sampling interval of 2 μs.

Figure 7. Equipment used for the in-situ asphalt seismic velocity measurement and operation.

The results for three calibration boreholes are presented. The seismic velocities measured for the asphalt are high, certainly caused by low temperature conditions. A minimum of four to six measurements were done on each site; table 1 presents the mean seismic velocities and their repeatability spans, corresponding to the standard deviation.

Table 1
Measured asphalt P wave velocities

		Span (± m/s)
BH-44	3494	198
BH-49	3909	100
BH-50	4035	176

A single piezoelectric receiver (50 kHz) was located at the borehole location to verify the accuracy of NDT sounding. The signal source was a compressed air pellet riffle to generate a seismic source frequency ranging between 25 and 35 kHz, which differs from the expected range of frequency related to the resonance of the asphalt layer to be clearly separated. Shots were repeated every 10 cm, from 10 cm to 200 cm from the receiver. Conventional drill coring took place for the final calibration of asphalt thickness. Figure 8 presents a TISAR test carried on BH-50, and figure 9 shows the drill coring at BH-44.

Figure 8. TISAR test at BH-50.

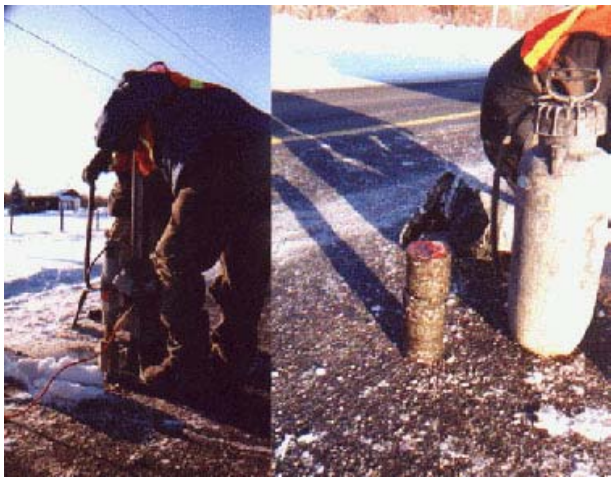

Figure 9. Conventional drill-coring at BH-44.

Seismograms can reveal the data quality, the occurrences of different wave types and it allows recognizing the time windows adequate for an adequate isolation of resonance signal (figure 10). Frequency analysis of the same data sets allows the identification of the seismic source frequency range and effective Tx-Rx range; the recognition of the characteristic signature associated with an increase of acoustic impedance with depth; and the optimal Tx-Rx offset window necessary for an appropriate isolation of the resonance signal (figure 11).

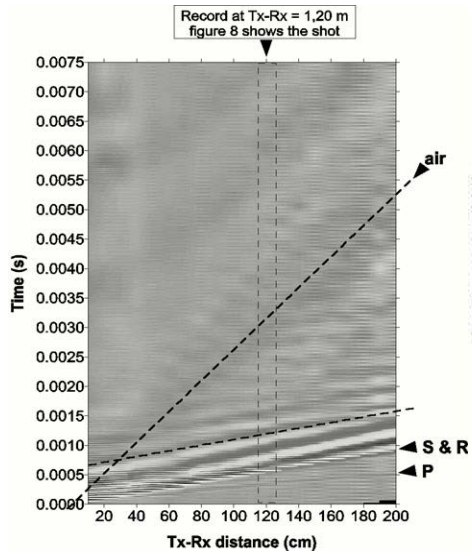

Figure 10. Seismogram (BH-50).

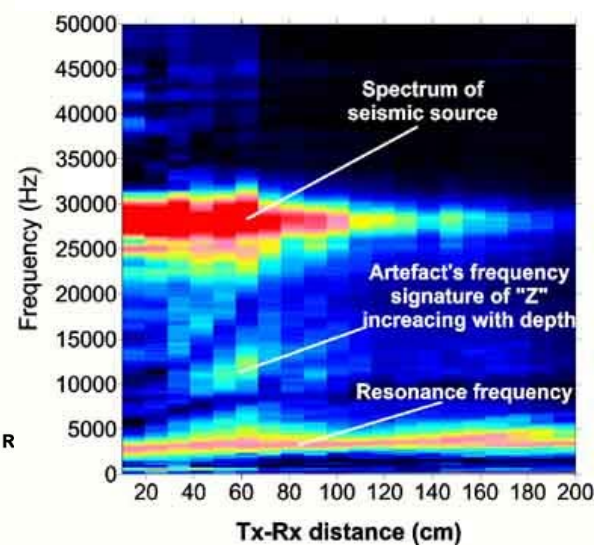

Figure 11. Spectrogram from seismogram (BH-50).

The drill-coring results indicate that asphalt thickness is 274 mm for BH-44, 260 mm for BH-49 and 270 mm for BH-50. From the Tx-Rx spectrograms presented at figure 12, one can observe the optimal Tx-Rx windows for a good identification of the resonance frequencies. Once the Tx-Rx windows are properly determined, we can isolate the frequency signals of interest, and stack them according to these distance limits. The resulting spectrograms can be transformed into depth responses using the general TISAR equation and the measured seismic velocities. It is possible to produce thickness models with confidence intervals. Figure 13 presents the converted depth responses for the TISAR (blue and green) and for the conventional impact-echo (black and grey). The red line indicates the asphalt thickness as measured from the recovered cores.

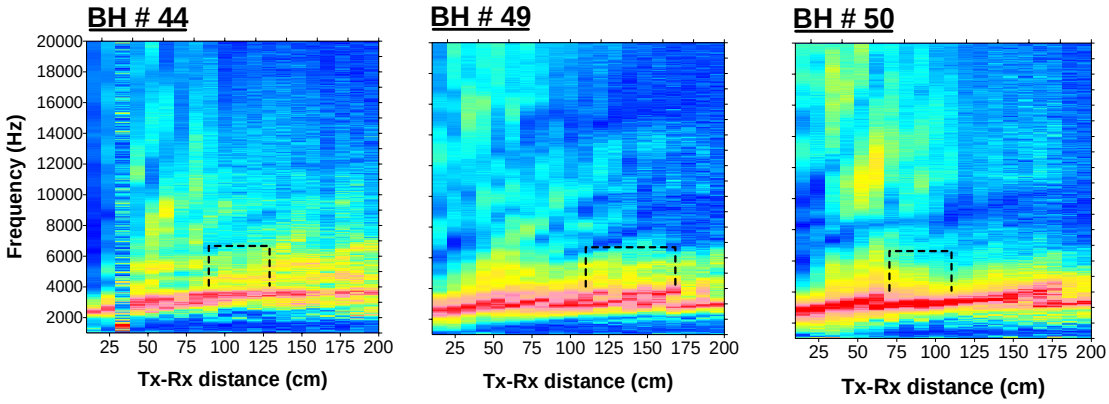

Figure 12. Tx-Rx spectrograms at BH-44, BH-49 & BH-50 and optimal windows.

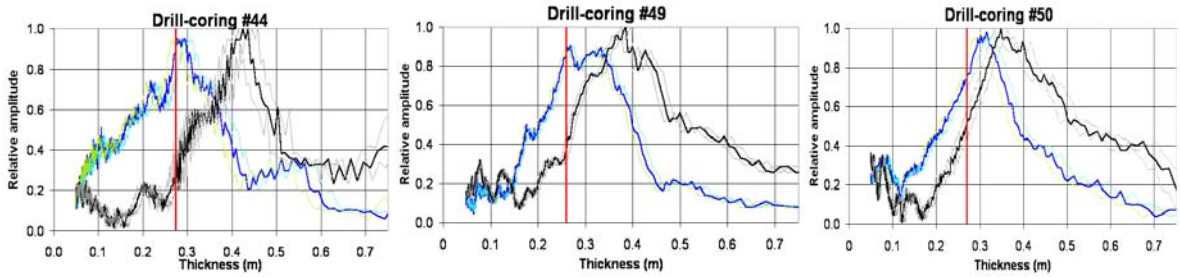

Figure 13. Asphalt thickness computed using acoustic resonance and impact-echo.

Figure 13 shows a good fit between the recovered core thicknesses and the TISAR results, while the ones from impact-echo present a bias leading to an overestimation of the thickness. A closer look at the TISAR results at BH-44 suggests that two interfaces could exist in the asphalt layer, at a depth of 0.10m and 0.21m. As illustrated on the picture of figure 14, the recovered core was broken at 0.103m from the surface. It can be associated to a weaken level within the asphalt layer. On the same picture, a dark and thin horizon can be noticed at the bottom of the core (0.207m depth). This is considered to be the interface between the old asphalt pavement and the more recent one.

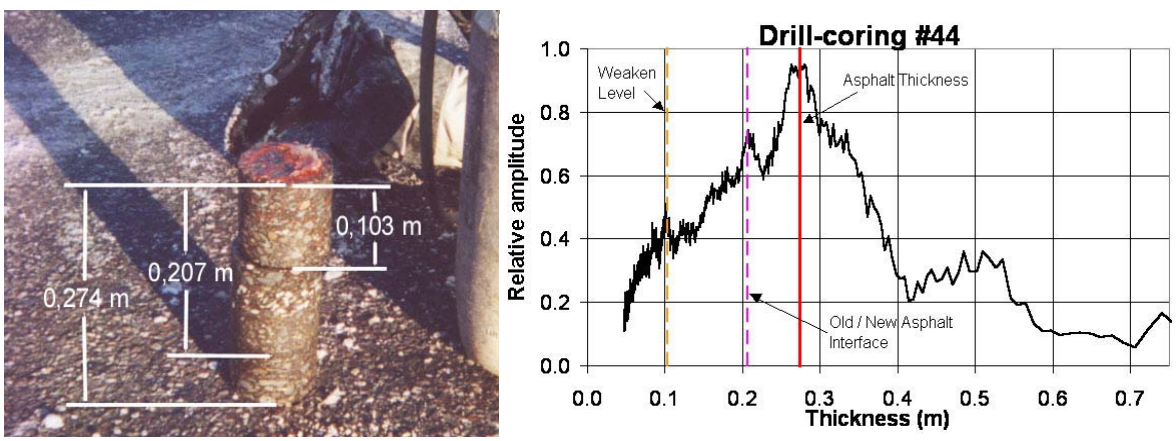

Figure 14. Details of the recovered core at BH-44 and TISAR data.

The TISAR survey on paved roads has yielded relatively accurate information. The high resolution of these results has also helped to locate some mechanical interfaces at depth which could not necessarily be detected from a radar survey and the method is completely non-destructive.

4.2-**Detection of Shallow Buried Utilities**

Detection of buried utilities is of interest before construction or restoration works take place, especially in urban areas. Even if ground-probing radar is often the first choice of engineers for the detection of shallow buried utilities, its application can be limited in some geological environments. Dependently of the geometry and the depth of the object to be located, the TISAR method could be an alternative when the radar EM signal cannot penetrate the soil.

We present two radar/TISAR comparative results for buried pipelines detection, one in sandy soil and the other in clay. According to modeling results, the TISAR could not directly locate a buried pipe at depth. It could only image subsurface changes caused by trenches.

4.2.1-**Detection of a gas pipe-line in sand**

A shallow buried gas pipeline was well located in a field, around 30 km North-East of Montreal. The general stratigraphy at this site consists of 0,2 – 0,5 m organic soil on surface, laying on a 3,5 m thick medium grained loose sand, followed by a 25 - 30 m thick clay deposit, a thin glacial moraine overlying bedrock (shale). The water table takes place into the loose sandy layer. The gas pipeline is located on the surface by numerous stakes posted by the gas company. The pipeline (3 feet in diameter) is supposed to be buried at a depth of 2 m, and protected by a concrete slab on top.

A conventional radar survey was carried over the expected pipeline with a Pulse Ekko IV system (Sensors & Software inc. Mississauga, ON) and a pair of 100 MHz antennas. Figure 15 displays the radar section and the classic hyperbola signature associated with a pipe.

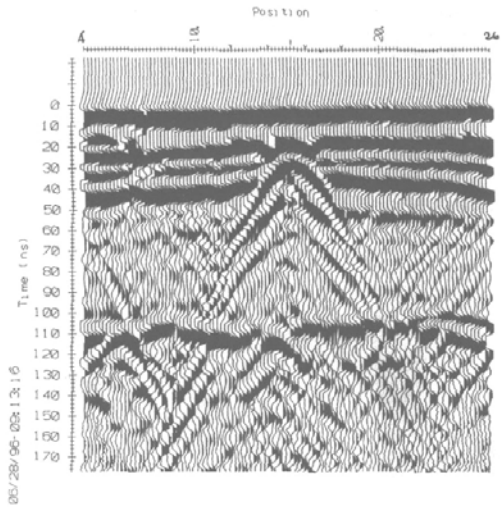

Figure 15. Typical radar hyperbola associated with the pipeline.

A single string of 24 geophones (14 Hz) was spread over the expected target with a 0.5 m spacing. A conventional engineering seismograph (ABEM Mark VI) recorded the data and a sledgehammer striking a metal plate on surface was used. The seismic velocity of the material was measured from the seismograms recorded in a traditional seismic refraction manner(with a hammer strike). Using the seismic velocity measured, the resonogram was converted into a depth cross-section, as shown in figure 16.

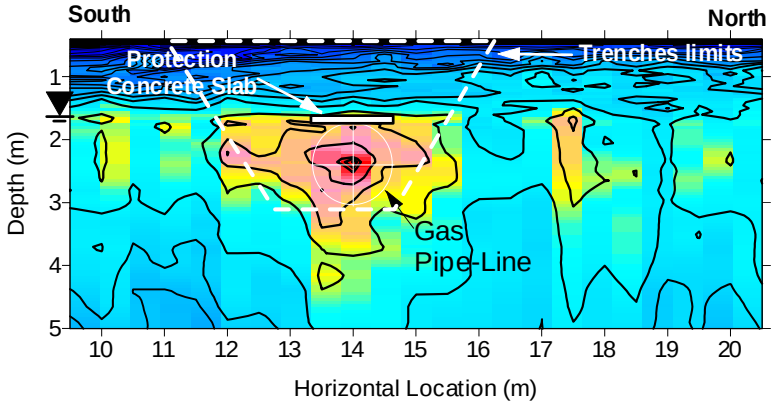

Figure 16. TISAR cross-section over the buried gas pipeline.

According with the installation details supplied by the gas company, the TISAR maps the excavation limits with a fuzzy representation. We believe that the clear pipeline location is due to the effect of the top protective concrete slab. One can also notice the resonance response associated with the water table (measured from three piezometers along the profile) at a depth of 1.7m.

Because of the sandy soil environment, locating the gas pipeline was easy and evident using a radar system. The TISAR survey was significantly slower but it led to good location estimates.

4.2.2- **Detection of a water pipe in clayey soil**

On the south shore of Montreal, the location of a shallow buried aqueduct was known from a city civil engineering drawing. The site stratigraphy is very simple as the fill material (soil, sand, cobbles and few small boulders) of around 1 m thick covers a clay layer (about 2 m) on altered shale. The aqueduct is almost 0.90 m in diameter, and should be about 1.5 to 2 m deep

A radar survey was performed using a SIR-10B (GSSI) with a 500 MHz antenna to accurately locate the aqueduct. Figure 17 shows the recorded radar section.

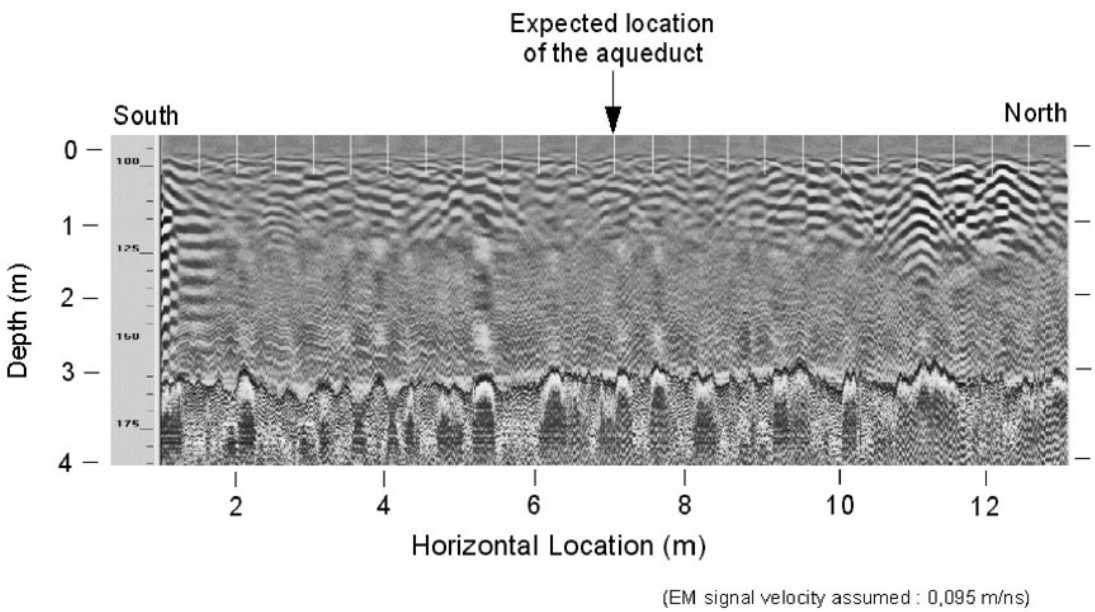

Figure 17. Processed (filtered) radar section over the aqueduct.

The upper fill material is easily displayed on the radar section. The EM signal was therefore absorbed in the top clay layer. Below 1 m, no signal is returned; the interface shown at 3 m deep is mostly a processing artifact. In this clayey environment, the use of radar appears to be useless as the aqueduct cannot be located neither the limits of the initial excavation to install the pipe.

A TISAR survey was then carried out over the expected aqueduct. The seismic acquisition system used was a conventional engineering seismograph (ABEM Mark VI) and three spreads of 24 geophones (14 Hz) with a 0,.2 m spacing. The seismic velocity of the material was measured from the recorded seismograms, in a traditional seismic refraction manner. Figure 18 shows the 1st and 2nd spread deployments over the expected aqueduct axis.

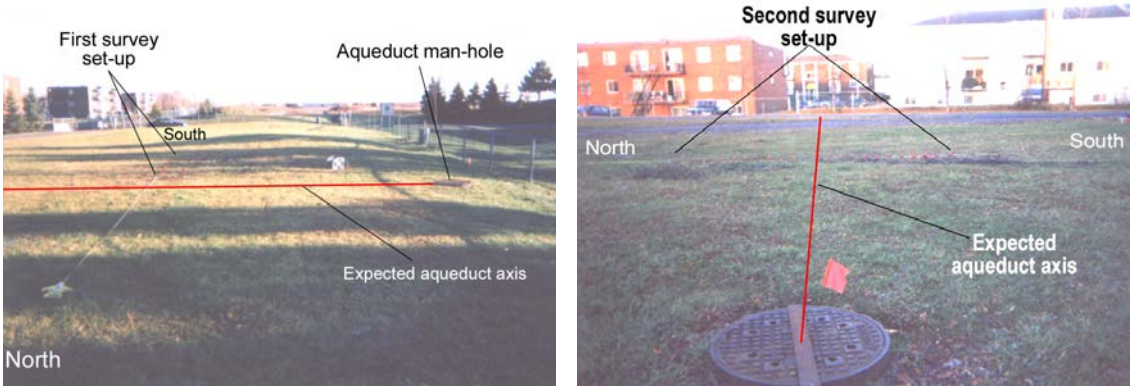

Figure 18. Field set-ups (1st and 2nd of 3) for TISAR acquisition.

The total of 74 geophones covered a 14,2m section, almost centered over the expected aqueduct axis. The signal source was a sledgehammer striking a metal plate on the ground surface every 2 m between locations –4 m and +14 m. The resulting resonogram was converted into a geological cross-section in accordance with the computed seismic velocities. Figure 19 displays the raw TISAR cross-section.

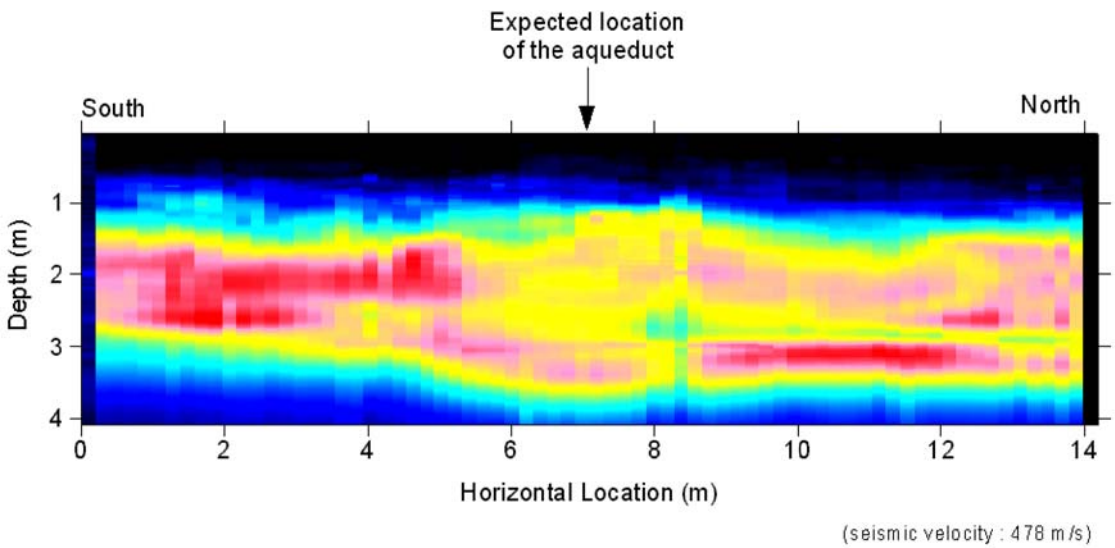

Figure 19. Raw TISAR geological cross-section over the aqueduct.

Without any image enhancement the figure 19 shows clearly the rock interface at 2,5 m deep on the South side and at 3,2 m deep in the middle and the North side. Moreover, the fill material / clay material interface is located at about 1,8 m deep, but it seems to be disturbed between the horizontal location of 6 and 10,5 m. According to the frequency signature, the aqueduct is interpreted to be located around the horizontal position of 7,5 m, instead of 7,0 m as expected from the 1:2500 engineering drawing. The accuracy of the drawing (±1,25 m) meets very well the response of the TISAR surveys. The aqueduct pipeline cannot be directly detected and located as expected from previous numerical analysis. The excavations material's alteration is whatever clearly expressed from the TISAR results, and a frequency signature associated to the aqueduct cylinder pipeline is also visible at figure 19.

The use of TISAR surveys permitted indirectly the location of the buried aqueduct, while the radar results offers absolutely no clues in this electrically conductive clayey environment. The TISAR technique

then appears as an alternative approach, giving mechanical information instead of electromagnetic ones. The TISAR results therefore remain constrained to continuous reflectors for an adequate illustration.

5- Conclusions

The late time part of the seismograms (usually rejected as “noise”) contains useful information related to resonance of the subsurface layers. Correct extraction of those resonant frequencies lead to direct estimation of layer thicknesses and indirect evaluation of the mechanical properties of material within the layers.

The TISAR method allows a mechanical profiling, or sounding, of the very shallow interfaces, which are not necessarily perceptible with EM methods such as radar. The experiment performed over asphalt paved road showed a very high resolution and sensitivity to mechanical characteristics of the layering within the material, which match very well with the observations from conventional drill-coring method, limiting the use of the destructive technique to just a few calibration holes. Tests for utility detection showed that the TISAR method could be an interesting alternative to GPR surveys when they are ambiguous or simply failed.

The TISAR method may play the role of a complementary method to GPR surveys to help/improve interpretation of the subsurface or an alternative to GPR in the cases where the latter is not applicable. The proposed method could also to allow complementing the conventional seismic reflection surveys, as they do not usually allow an adequate profiling of the sub-surface for the first 10 meters.

The proposed method is at an early stage of development; however it shows promising new avenues for NDT.

References

Abraham, O., Côte, P., Leonard, C., Piwakowski, B. and Shahrour, I.,1998, Application of the “impact echo method” to the detection of underground cavities. Part II : field experiments, Proc. of the EEGS, Barcelona, Spain, Sept., pp.347-350.

Arsenault, J.L. and Chouteau, M., 2001, Frequency analysis of seismic records for very shallow seismic profiling. Part I – Basic theoretical principles, Proc. of the EEGS, Birmingham, U.K., Sept., pp.240-241.

Arsenault, J.L. and Chouteau, M., 2001, Frequency analysis of seismic records for very shallow seismic profiling. Part II – Application to modeled and survey data, Proc. of the EEGS, Birmingham, U.K., Sept., pp.248-249.

Leonard, C., 2000, Détection des cavités souterraines par sismique haute résolution et par Impact-Écho, Ph.D. thesis, Université des Sciences et Technologies de Lille, 178 p.

Leonard, C., Piwakowski, B., Shahrour, I., Abraham, O. and Côte, P.,1998, Application of the “impact echo method” to the detection of underground cavities. Part I : theory and finite element modeling, Proc. of the EEGS, Barcelona, Spain, Sept., pp.343-346.

Lin, Y. and Sansalone, M., 1992, Transient response of thick rectangular bars subjected to transverse elastic impact, J. Acoust. Soc. Am., **Vol. 91**, No. 4, pp.2674-2685.

Lin, Y. and Sansalone, M., 1994, Impact-Echo Response of Hollow Cylindrical Concrete Structures Surrounded by Soil and Rock: Part I – Numerical Studies, Geotechnical Testing Journal, GTJODJ, **Vol. 17**, No. 2, pp.207-219.

Skudrzyk, E., 1971, The Foundations of Acoustics, Basics Mathematics and Basics Acoustics, Springer-Verlag, New-York, 790 p.